Constraints on MOND from the lensing cluster MS2137-23

Raphael Gavazzi

Constraints on MOND from the lensing cluster MS2137-23

R. Gavazzi [a]

[a] *Institut d'Astrophysique de Paris, 98bis Boulevard Arago, 75014 Paris, FRANCE*

Abstract

The cluster of galaxies MS2137-23 presents the most constrained lensing configuration of gravitational images ever detected in a distant cluster of galaxies. With a set of two arc systems with known redshifts and many other arclets spread between $\approx 30\ h^{-1}$ kpc and $1\ h^{-1}$ Mpc, MS2137-27 is well suited to probe its mass profile and to challenge theoretical expectations from CDM scenario with more speculative alternatives, like MOND models. In this note, I describe the recent lensing analysis I carried out on this cluster using together arcs and CHANDRA X-ray data. Even with this unique data set, I cannot reject neither an isothermal model nor an NFW model. The MOND model is not compatible with the observations, unless a significant fraction of the baryonic matter has not been detected by CHANDRA. The need for much more baryons in the MOND model than for the dark matter paradigm implies significant dynamical differences between these models which can be explored at very large radial distance. In particular, MOND lensing signal becomes isotropic beyond $1\ h^{-1}$ Mpc, in contrast with collisionless DM halos which produce elliptical potentials. This difference can in principle be used to test MOND prescriptions, regardless the exact relation between matter and the gravitational deflection law assumed for MOND.

Key words: Dark Matter, Strong Lensing, clusters of galaxies, Cluster, individual : MS2137-23, MOND

1 Introduction

Numerical simulations (Navarro, Frenk, & White, 1997), in the CDM paradigm, predict that dark matter halos follow a universal density profile. The profile property depends on cosmological parameters, the redshift of the system and its total mass. However, density profiles as simple as isothermal

Email address: gavazzi@iap.fr (R. Gavazzi).

spheres are still consistent with observations. The peculiar case of flat rotation curves in spiral galaxies first motivated the introduction of isothermal dark matter halos. However, these observations are also explained in the MOND framework by modifying Newtonian gravity in the limit of weak accelerations ($a < a_0 \sim 1.2\,10^{-8} cm.s^{-2}$). Under this assumption, beyond a critical limiting radius r_m depending on the system mass, gravitational interaction scales as r^{-1}. Hence, in the MOND context, flat rotation curves are simply explained without the need of exotic dark matter. Such a behavior has strong consequences, in particular for lensing.

Because gravitational lensing probes projected gravitational potential without regard on the nature of the various deflecting mass components, it is in principle an interesting tool to explore alternative theoretical models, like MOND. If clusters of galaxies, through strong and weak lensing models, are constrained enough to produce accurate potential reconstructions over a wide radial range, one can make strong statements on gravity theories or the dark matter distribution properties. MOND phenomenology is still unable to arise from an auto-consistent relativistic geometrical theory but, as General Relativity which predicts a deflection angle twice the Newtonian value, MONDian lensing formalism generally assumes the same relation. The MOND representation of lensing in structures gives the same results as isothermal DM halos, as in rotation curve modeling. The more evident way to reject MOND is therefore to probe discrepancies between the observable baryonic matter distribution and the gravitational mass properties, like its geometry or its total mass.

The lensing cluster of galaxies MS2137-23 (Fort et al., 1992) is an interesting candidate to explore the properties of its gravitational potential on scales ranging from $1\,kpc$ to $1\,Mpc$. This cluster shows multiple strongly distorted images (a tangential arc lying at $\sim 100\,kpc$, a rare radial arc at $\sim 20\,kpc$) near the center. The position and the shape of these arcs are well constrained by high-resolution HST images, while weak lensing analysis can be carried out thanks to new very deep and multi-color VLT/FORS observations ($r \leq 1\,Mpc$). This X-ray emitting cluster has also recently been observed with CHANDRA (Allen, Schmidt, & Fabian, 2002) and appears to be well relaxed. Join together, lensing, optical and X-ray data permit to build the most constrained lensing model ever done for a distant cluster of galaxies. I discuss these models in the contexts of CDM scenario as well as a MOND interpretation.

In this paper, I assume a $\Omega_m = 0.3,\ \Omega_\Lambda = 0.7,\ H_0 = 100\ h\ km.s^{-1}.kpc^{-1}$ cosmology.

2 Gravitational lensing in Newtonian-GR versus MOND gravity

The bending of a light-ray by a matter distribution located between a source and the observer can be expressed by a transformation between a source plane point and its corresponding image in the lens plane:

$$\vec{\theta_s} = \vec{\theta_i} - \vec{\nabla}_{\theta_i}\phi(\vec{\theta_i}) \tag{1}$$

where ϕ is the 2D projected lens gravitational potential, in units of $\frac{2}{c^2}\frac{D_{ol}D_{ls}}{D_{os}}$, with D_{ol}, D_{ls} and D_{os} are respectively the observer-lens, lens-source and observer-source angular distances.

Locally, the transformation Jacobian defines the useful quantities :

$$\mu^{-1} = \begin{pmatrix} 1-\partial_{xx}\phi & -\partial_{xy}\phi \\ -\partial_{xy}\phi & 1-\partial_{yy}\phi \end{pmatrix} = \begin{pmatrix} 1-\kappa-\gamma_1 & -\gamma_2 \\ -\gamma_2 & 1-\kappa+\gamma_1 \end{pmatrix}. \tag{2}$$

κ is the gravitational convergence, such that $\nabla^2\phi = \frac{1}{2}\kappa$ measures the isotropic beam deformation. $\gamma = \gamma_1 + i\gamma_2$ is the complex shear which measures the anisotropic term, or the gravitational distortion. $\det[\mu]$ is the magnification relating a surface element in the source plane to its image.

In the Newton theory, the potential is always related to the mass density through the Poisson equation ($\nabla^2\Phi = 4\pi G\rho$). Once projected along a line of sight it writes

$$\nabla^2\phi = \frac{1}{2}\kappa \stackrel{def}{=} \frac{1}{2}\frac{\Sigma}{\Sigma_{crit}}, \tag{3}$$

where Σ is the projected surface density and Σ_{crit} is defined as the critical surface density $\Sigma_{crit} = c^2/(4\pi G)D_{os}/(D_{ls}D_{ol})$.

In the MOND theory, the gravitational acceleration is modified :

$$\mu(g/a_0)\, g = -\frac{GM(r)}{r^2} \tag{4}$$

with $\mu(x) = 1$ when $x \gg 1$ and $\mu(x) = x$ when $x \ll 1$. Thus, the Poisson equation cannot be expressed easily. It is also difficult to express its 2D projection because of the non-local relation between mass and potential. However, as for rotation curve of galaxies, in a MOND description gravitational lensing can be described as in General Relativity (GR), by adding a massive

component (dark halo) with a slope $\rho(r) \propto r^{-2}$. Hence, MONDian lensing can be expressed in terms of the conventional formalism, if an "effective" surface density is defined. When expressed by either $\rho_N(r)$ or $\Sigma_N(R)$, it is the density profile that would, under the assumption of Newtonian mechanics, produce both the same rotation curve and the same deflection law as the MOND predictions. Given that a point-mass has an asymptotically constant rotation velocity of $v_c = (GMa_0)^{1/4}$ in MOND, the addition of an isothermal component, such that

$$\rho_N(r) \simeq \rho(r) + \sqrt{\frac{a_0\, M(r)}{G}} \frac{1}{4\pi r^2}, \tag{5}$$

as a reasonable approximation to many MONDian deflectors of true mass M.

Through this relation, it is possible to interpret our analysis in terms of MOND, rather than assuming dark matter. If so, only a baryonic mass component should be able to fit the density ρ of Eq.(5), with the parameters deduced from a lensing + X-ray analysis.

3 Cluster of galaxies MS2137

3.1 Observations

MS2137-23 is a rich cD cluster of galaxies located at $z_l = 0.313$. The innermost region (< 5') does not show any substructures and has regular visible appearance, as expected for a dynamically relaxed gravitational system. A single dominant cD galaxy occupies the central region. Optical data provide its azimuthal light distribution and show that its diffuse light component is almost elliptical. The stellar component reveals a small twist of the isophotes' orientation between the radial and tangential arcs. From North to East, the position angle is $PA \simeq (71 \pm 4)^\circ$.

The lens generates a tangential arc (A01-A02) associated with two other counter-images A2 and A4 positioned around the cD galaxy. A01 and A02 are twin image with reverse parity. They are two merging "partial" images of the source element located inside the tangential caustic line. A non-singular potential should create a fifth demagnified image located near the center. The cD galaxy brightness peak hampers its detection without a complex image subtraction.

The lens also gives rise to a radial arc A1 partially embedded in the cD stellar diffuse component. This arc is associated with a bright image, referenced as

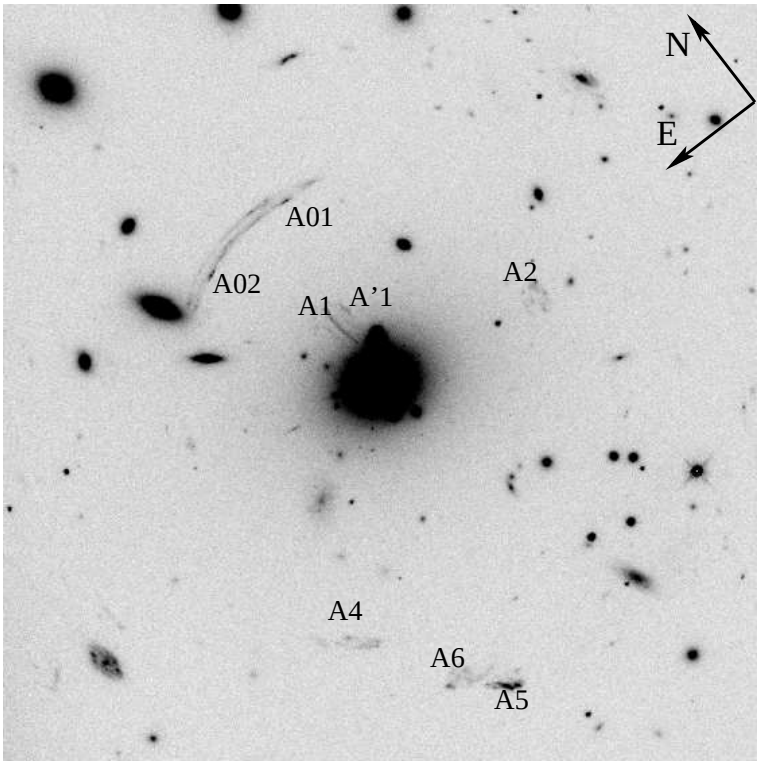

Fig. 1. *Overview of the lensing configuration. The three arcs systems {A01,A02,A2,A4}, {A1,A5} and {A'1,A6}. The central cD galaxy. This F702 HST field is* 56×56 *arcsec wide.*

A5. As explained by Hammer et al. (1997), the diffuse objet A6 near A5 is probably another counter-arc associated to the diffuse object A'1 located close to the radial arc A1. This configuration is possible only if the {A6,A'1} redshift is significantly lower than {A1,A5}.

New wide field multiband VLT data (see Gavazzi et al (2002) for a detailed description) were used to get the photometric redshift of arcs : both radial and tangential arcs turn out to be at $z_s \simeq 1.61 \pm 0.05$.

Recent CHANDRA observations of MS2137 (Allen, Schmidt, & Fabian, 2002) provide important new constraints on the halo density profile. The authors confirm its apparent relaxed shape, but pointed out the presence of a strong cooling flow inside the innermost region. Thus, a simple isothermal parameterization of the dark matter profile, assuming hydrostatic equilibrium probably over-simplifies the central potential well. Allen, Schmidt, & Fabian (2002) modeled the X-ray emission and derived a gas mass fraction $f_{gas} \simeq 0.11$ which is almost constant between 10 and 100 arcsec. The MS2137 radial properties inferred from X-rays data reveal that the luminosity profile presents a $r_c \approx 7$ arcsec core radius and an asymptotic slope $\alpha \sim 1.17$ consistent with isothermal profile for dark matter and a $\beta \sim 0.61$ index. The X-isophotes are remarquably elliptical and do not show substructures. The orientation of gas is

almost constant : $PA_X = 58° \pm 7°$, except a sharp isophotal twist inside 7 arcsec from the center (where ellipticity looses meaning and orientation is difficult to determine). A comparison of the stars and intra-cluster gas distributions is represented in 2. A new characteristic feature is the global misalignment between diffuse stellar component and hot intra-cluster gas. This result suggests that the light distribution does not match exactly the DM distribution. This point is confirmed by strong lensing models which are detailed in the next section.

3.2 Strong lensing modeling

The lens is modeled by two different types of mass distributions : a softened elliptical isothermal profile, or an elliptical NFW universal profile of the form $\rho(r) = \frac{\rho_c(z)\delta_c}{r/r_s(1+r/r_s)^2}$ projected in $\kappa(r) = 2\kappa_s \frac{1-F(r/r_s)}{(r/r_s)^2-1}$ [1]. Both are consistent with arcs observations with a comparable χ^2. Results are summarized in table 1. Free parameters are respectively (central velocity dispersion σ_v, core radius r_c) and (κ_s, r_s), ellipticity ϵ and position angle θ_0. We first centered the potential on the center of the cD galaxy. This assumption is verified a posteriori by relaxing its position around the first best fit models. The $95.5\% CL$ allowed distance to the cD center is less than 1 kpc.

NFW	isothermal (isoT)
$\kappa_s = 0.6 \pm 0.2$	$\sigma_v = 1015 \pm 16\, km/s$
$r_s = 80 \pm 10\, h^{-1}\, kpc = 25 \pm 4\,''$	$r_c = 11 \pm 2\, h^{-1}\, kpc = 3.3 \pm 0.5\,''$
$\Rightarrow \begin{cases} c = 11.7 \pm 2.1 \\ r_{200} = 940 \pm 200\, h^{-1}\, kpc \end{cases}$	
$\epsilon = 0.24 \pm 0.01$	$\epsilon = 0.23 \pm 0.01$
$\theta_0 = 57.4° \pm 0.8°$	$\theta_0 = 58.4° \pm 1.0°$

Table 1
Final models. Einstein radius is the same in the two best models : $R_E = (18.0 \pm 1.3)\, arcsec = (58 \pm 4)\, h^{-1} kpc$. *For both, the total mass inside is* $M(r < R_E) = (3.9 \pm 0.5) 10^{13}\, h^{-1} M_\odot$.

As (Mellier et al., 1993; Hammer et al., 1997) argued, the isothermal profile core radius is necessarily finite, otherwise a constant $\alpha = 2$ slope is inconsistent with radial arcs. The NFW model is however slightly more concentrated than numerical ΛCDM predictions. This might results from complex dissipative cooling of baryons inside the core of the cluster which pulled down the matter. On those scales, the physics of each matter component is hard to with present-day resolution of numerical simulations. (For a more detailed discussion, see

[1] $F(x) = \begin{cases} \frac{1}{\sqrt{x^2-1}} \tan^{-1} \sqrt{x^2-1} & for\ x > 1 \\ \frac{1}{\sqrt{1-x^2}} \tanh^{-1} \sqrt{1-x^2} & for\ x < 1 \\ 1 & for\ x = 1 \end{cases}$

Gavazzi et al (2002). See also e.g. Blumenthal et al (1986); Keeton (2001))

Nevertheless, figure 2 reveals discrepancies outside the cluster area probe by the radial and the tangential arc. The use weak lensing discussed in the next section can help to probe the mass profile on larger scale. In the innermost region, the expected discrepancies between both models can be tested by looking for the fifth demagnified image associated to the tangential arc system {A01,A02,A2,A4}. Unfortunately, because it is demagnified by a factor 5 (resp. 10) in the isothermal (resp. NFW) model, the cD stellar light peak hampers its detection. We used a spatial high-bandpass filtering to remove the diffuse cD component. Then using together color indications, we find a marginal detection of this image at the location expected by isothermal and NFW models. This detection is however not conclusive. In the future, high resolution in narrow-band filter spectro-imagery should confirm/reject the detection and should provide important constraints regarding the central cusp/core problem in dark matter profiles.

The potential inferred from strong lensing shows the same misalignment ($\Delta\varphi = 13° \pm 4°$) as X-ray isophotes with respect to the diffuse stellar component of the cD galaxy. This asymmetry may provide interesting clues about the MOND models against the dark matter paradigm. If baryons are the only source of gravity, the potential must show the same azimuthal symmetry. In contrast, this symmetry requirement is not needed for dark matter halos. It is therefore interesting to see that, as it stands from the lens model, the geometry of the hot baryonic contribution does not rule out the MOND model.

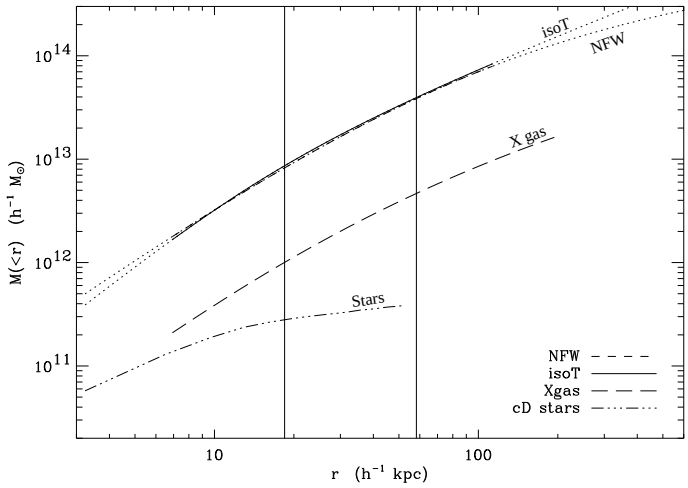

Fig. 2. *Various mass contributions in the cluster center. Stellar contribution is deduced from the I band luminosity profile (with an applied K-correction of 0.23 and a mass-to-light ratio of $\Upsilon_I = 2$). Hot gas contribution arises from (Allen, Schmidt, & Fabian, 2002). Upper curves result from the strong lensing modeling. Right vertical line indicates the Einstein radius, the left one the radial arc position.*

3.3 Weak lensing analysis

The new VLT photometry allowed us carry out a weak lensing analysis of MS2137-23 and to reconstruct its mass map over the whole FORS $7'30 \times 7'30$ field around the cD galaxy. Multiband UBVRI and VLT/ISAAC JK images were used to build a catalogue of background with an accurate photometric redshift information (Pelló et al., 2001). The mass map shows that the potential keeps the orientation and the shape inferred from the strong lensing model far beyond 1 arcmin from the center. In order to check the validity of the strong lensing models, we compute the ζ-statistic to measure the azimuthaly-averaged radial profile.

The ζ-statistic is derived from the measurement of individual tangential ellipticity of galaxies (averaged inside annuli to reduce the noise introduced by intrinsic ellipticity of galaxies). It is defined by

$$\zeta(r) = \bar{\kappa}(r' < r) - \bar{\kappa}(r < r' < r_{out}) \tag{6}$$

With this definition, beyond the radius r_{out}, the density is assumed to drop significantly. Due to the mass-sheet degeneracy, the projected mass profile is only known through the invariance transformation $(1-\kappa) \rightarrow \lambda(1-\kappa)$ (see e.g. Schneider, Ehlers, & Falco (1992)). From the definition of $\zeta(r)$, only a lower limit of the total mass given by $\pi r^2 \zeta(r) \Sigma_{crit}$ is available, where $\Sigma_{crit} = \frac{c^2}{4\pi G} \left\langle \frac{D_{ls} D_{ol}}{D_{os}} \right\rangle^{-1}$ (averaged over the sample redshift distribution).

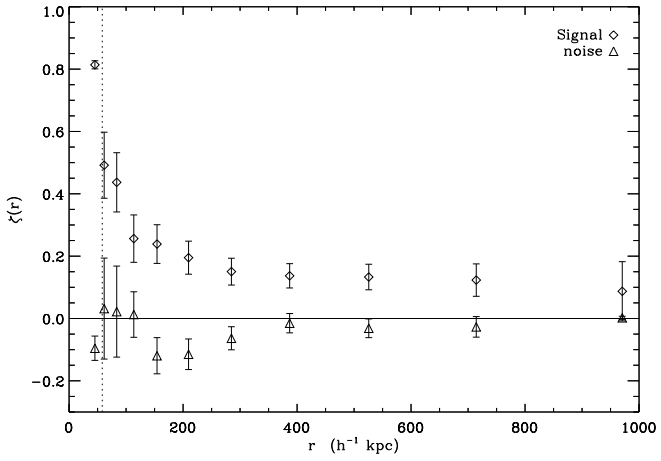

Fig. 3. *ζ-statistic result for MS2137. Diamonds represent the true signal. Triangles represent the same analysis after a $\pi/4$ rotation of all galaxies to only reveal noise. Vertical dotted line indicates the Einstein radius.*

The discrepancies between strong lensing and weak lensing (see fig 4) are very small. Thus, the global lensing mass looks robust. The model an be improved

by a full maximum likelihood parameterized analysis of the weak lensing sample, but it will not change the conclusions. Except at large radius, the weak lensing profile is consistency with both an isothermal or a NFW model. Beyond 600 h^{-1} kpc, the isothermal model seems favoured, but uncertainties produce by systematics (PSF anitropy corrections) make the two last points more questionnable. Note that before rejecting NFW profiles, one should include the "adiabatic" contraction influence of baryons modifying universal profiles and prohibiting a simple analytic fit on the whole radial range.

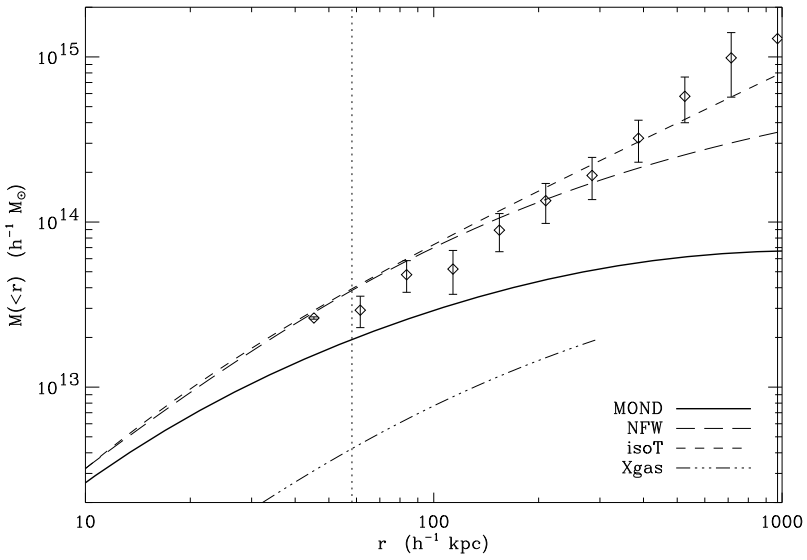

Fig. 4. *Various mass contributions in the cluster intermediate scales. Upper curves result from the two strong lensing models of table 1. Overplotted the weak lensing mass estimate (diamonds). One can see the good agreement between strong and weak lensing near the Einstein radius (dotted vertical line). (thick) MOND baryonic mass profile inferred to explain both strong and weak lensing signal.*

4 Discussion in MOND framework & conclusion

A detailed review on lensing in the MOND theory can be found in (Mortlock et al., 2001a,b; Qin et al, 1995). For the purpose here, we only use equation (5) to calculate the MOND baryonic mass distribution known the isothermal DM halo profile needed in Newtonian grativy to explain multiple arcs, and consequently weak lensing signal.

By inverting relation (5) we find the MOND baryonic mass profile shown in figure 4. The mass discrepancy between the observed X-ray emitting gas and the MOND prediction put the MOND model in a difficult position. However, one could imagine that some massive cold gas contributes to 3 times the observed hot gas inside 200 kpc, and even more than 5 times inside 50 kpc.

A similar problem has already been noticed in previous studies of X-ray clusters. But it refers to X-ray analyses assuming isothermality and hydrostatic equilibrium of the gaz, which is not the case here. Note that even with a baryonic content 3 times larger than the hot X-ray component, the MOND-expected central amount of gas does not to contradict the baryon fraction predicted by the Big Bang Nucleosynthesis, because beyond $\sim 1\,Mpc$ the baryonic mass is almost constant. This mass corresponds to an homogeneous collapse of a sphere of canonical radius $r \sim 20\,h^{-1}\,kpc$, with density $\Omega_b h^2 \sim 0.03$.

One can assume that the missing gas fraction exists under a cooler phase, as suggested by observed cooling flows or under an unknown other form. Such an amount of central high-density gas could be tested by its consequencies on the fifth demagnified image in the near future when high spatial resolutions observations will be available.

The analysis of MS2137-23 illustrates how one can use observations of lensing clusters to challenge modified gravity theories against orthodox dark matter scenario. We show that isothermal profiles and consequently MOND are consistent with the whole constraints on the range $10\,kpc \lesssim r \lesssim 1\,Mpc$. However, MOND models overpredict baryonic mass observed from the hot X-ray-emmitting ICM phase. A more promising lensing test for MOND phenomenology is given in Hoekstra et al. (this proceeding) concerning galaxy-galaxy lensing and particularly, large scale potential symmetry with regards to the observable matter distribution. MOND predicts an isotropic lensing signal far enough from baryonic concentrations, independently of the exact radial relation potential-mass distribution.

We thank the organizers for the invitation and B. Fort and Y. Mellier for fruitfull discussions and careful reading of this research note.

References

Allen, S. W., Schmidt, R. W., & Fabian, A. C. 2002, *MNRAS*, 334, L11

Blumenthal, G. R., Faber, S. M., Flores, R., & Primack, J. R. 1986, *ApJ*, 301, 27

Fort, B., Le Fevre, O., Hammer, F., & Cailloux, M. 1992, *ApJl*, 399, L125

Gavazzi, R., Fort, B., Mellier, Y., Dantel-Fort, M., Pelló, R. 2002, in preparation.

Hammer, F., Gioia, I. M., Shaya, E. J., Teyssandier, P., Le Fevre, O., & Luppino, G. A. 1997, *ApJ*, 491, 477

Keeton, C. R. 2001, *ApJ*, 561, 46

Navarro, J. F., Frenk, C. S., & White, S. D. M. 1997, *ApJ*, 490, 493

Mellier, Y., Fort, B., & Kneib, J. 1993, *ApJ*, 407, 33

Milgrom, M. 1983, *ApJ*, 270, 371

Milgrom, M. 1999, Dark matter in Astrophysics and Particle Physics, 443
Mortlock, D. J. & Turner, E. L. 2001, *MNRAS*, 327, 557
Mortlock, D. J. & Turner, E. L. 2001, *A&A*, 327, 552
Pelló, R. et al. 2001, Astrophysics and Space Science Supplement, 277, 547
Qin, B., Wu, X. P., & Zou, Z. L. 1995, *A&A*, 296, 264
Schneider, P., Ehlers, J. ;., & Falco, E. E. 1992, Gravitational Lenses, XIV, 560 pp. 112 figs.. Springer-Verlag Berlin Heidelberg New York. Also Astronomy and Astrophysics Library,